Available online at www.sciencedirect.com
SCIENCE DIRECT®
ELSEVIER
International Journal of Plasticity 22 (2006) 1432–1455
INTERNATIONAL JOURNAL OF Plasticity
www.elsevier.com/locate/ijplas

Randomness and slip avalanches in gradient plasticity

Michael Zaiser [a], Elias C. Aifantis [b,c,*]

[a] *The University of Edinburgh, Institute for Materials and Processes, The King's Buildings, Sanderson Building, Edinburgh EH11DT, UK*
[b] *Aristotle University of Thessaloniki, Laboratory of Mechanics and Materials, Polytechnic School, Box 468, 54124 Thessaloniki, Greece*
[c] *Michigan Technological University, Center for the Mechanics of Material Instabilities and Material Processes, Houghton, MI 49931, USA*

Received 1 September 2004
Available online 28 February 2006

Abstract

While localization of deformation at macroscopic scales has been documented and carefully characterized long ago, it is only recently that systematic experimental investigations have demonstrated that plastic flow of crystalline solids on mesoscopic scales proceeds in a strongly heterogenous and intermittent manner. In fact, deformation is characterized by intermittent bursts ('slip avalanches') the sizes of which obey power-law statistics. In the spatial domain, these avalanches produce characteristic deformation patterns in the form of slip lines and slip bands. Unlike to the case of macroscopic localization where gradient plasticity can capture the width and spacing of shear bands in the softening regime of the stress–strain graph, this type of mesoscopically jerky like localized plastic flow is observed in spite of a globally convex stress–strain relationship and may not be captured by standard deterministic continuum modelling. We thus propose a generalized constitutive model which includes both second-order strain gradients and randomness in the local stress–strain relationship. These features are related to the internal stresses which govern dislocation motion on microscopic scales. It is shown that the model can successfully describe experimental observations on slip avalanches as well as the associated surface morphology characteristics.

Keywords: Material instabilities; Slip localization; Gradient plasticity; Avalanches

* Corresponding author. Fax: +30 310 995921.

0749-6419/$ - see front matter © 2006 Elsevier Ltd. All rights reserved.
doi:10.1016/j.ijplas.2005.07.010

1. Introduction and background

The characterization of plastic instabilities and associated deformation localization phenomena has been a challenge for the development of appropriate constitutive models for many years. This is because localization commonly occurs and subsequently evolves in the material softening regime, where the slope of the stress–strain graph is negative and the corresponding boundary-value problem is ill-posed leading, among other things, to non-uniqueness, non-convergence and mesh-size dependence of the solution in finite element calculations. The necessity to formulate constitutive equations which lead to mathematically well-posed boundary-value problems in the material softening regime, has motivated the development of gradient plasticity models as introduced by Aifantis and co-workers (e.g., Aifantis, 1984, 1987, 1992, 1995, 1996, 1999, 2001, 2003; Triantafyllidis and Aifantis, 1986; Zbib and Aifantis, 1988, 1989, 1992, 2003; Muhlhaus and Aifantis, 1991; Vardoulakis and Aifantis, 1991; Charalambakis and Aifantis, 1991; Oka et al., 1992, 2000; Zaiser and Aifantis, 1999; Zaiser and Aifantis, 2003a,b; Voyiadjis et al., 2001; di Prisco et al., 2002; Frantziskonis and Aifantis, 2002). Other researchers have contributed to gradient plasticity along similar or slightly different lines including Fleck and Hutchinson (1993, 1997, 2001), Fleck et al. (1994), Gao et al. (1999), Huang et al. (2000), Menzel and Steinmann (2000); Gurtin (2000, 2002), Gudmundson (2004), Fleck and Willis (2004), Aifantis and Willis (2004, 2005). Some authors (e.g., Maugin and Muschik, 1994; Polizzotto and Borino, 1998) have elaborated on formal thermodynamic aspects of gradient plasticity, while Valanis (1996, 1998a,b, 2000) provided such a thermodynamic framework to describe material instabilities and associated deformation patterning phenomena. From the viewpoint of materials science, the introduction of gradient terms into macroscopic constitutive equations is necessitated by the fact that the loss of macroscopic stability of deformation is intimately connected with the development of spatial heterogeneity, which is often governed by the presence of characteristic internal length scales in the microstructure of deforming materials. The relation between gradient terms and microstructural length scales has been demonstrated in many cases, and a standard example is the proportionality between shear band widths and grain sizes in polycrystals (e.g., Zbib and Aifantis, 1992; Aifantis, 1995). While spatial couplings may be governed by different mechanisms (for an overview, see e.g., Kubin et al., 1993) depending on materials and deformation conditions, it is now generally accepted that the introduction of gradient terms in the constitutive equations is an adequate and physically motivated means dealing with the problem of deformation localization in unstable plastic flow.

However, deformation heterogeneity and slip localization are not necessarily associated with, and/or may not always lead to macroscopic deformation instabilities. On the microscopic scale, slip localization is a trivial consequence of the discreteness of defects. For instance, in crystalline solids the Burgers vectors of dislocations which carry the plastic deformation define discrete 'quanta' of slip. Slip localization phenomena which take place in spite of macroscopically stable deformation may also be observed on mesoscopic scales where they involve the collective dynamics of very large numbers of elementary defects. A classical example is the formation of slip lines or slip bands in crystalline solids deforming by planar slip (for an overview of experimental observations, see Neuhäuser, 1984). The slip steps on the surface of these materials manifest the collective motion of large numbers of dislocations, leading to an intense but highly localized deformation heterogeneity there, in spite of the fact that macroscopic deformation is smooth and homogeneous. It has been

shown by different authors that slip patterns exhibit long-range spatial correlations which can be described in terms of fractal statistics (Kleiser and Bocek, 1986; Zaiser et al., 2001a; Weiss and Marsan, 2003). The relationship between the fractal nature of slip and the surface morphology of plastically deformed crystals has been discussed by Zaiser et al. (2004), who demonstrated that the surface of plastically deformed Cu samples develops self-affine roughness over several orders of magnitude in scale. The applicability of wavelet analysis and neural networks for characterizing the organization of slip at different scales has recently been demonstrated by Konstantinidis and Aifantis (2002).

Heterogeneity of slip in spite of macroscopically stable deformation is illustrated in Figs. 1–3. Fig. 1 shows surface profiles of a Cu polycrystal with an initially flat surface (rms roughness <2 nm as determined by atomic force microscopy over an area of 6×6 μm) after deformation to 9.6% tensile strain. The statistically self-affine nature of the profiles can be inferred by comparing profiles taken on different scales: here by atomic force microscopy (AFM, profile length 25 μm) and scanning white-light interferometry (SWLI, profile length 2 mm). A quantitative measure of self-affinity is the so-called Hurst exponent H: For a self-affine profile $y(x)$ the average height difference $\langle |y(x) - y(x+L)| \rangle$ increases like L^H (see Fig. 2). The Hurst exponent relates to the fractal dimension (box dimension) D_B of the profile via $D_B = 2 - H$. Zaiser et al. (2004) find that the fractal dimension of surface profiles from deformed Cu samples increases within the first few

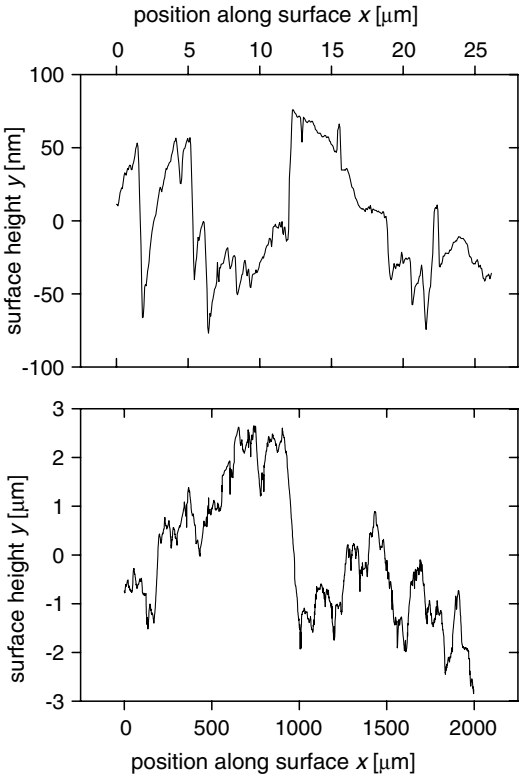

Fig. 1. Surface profiles of a Cu polycrystal deformed in tension to a plastic strain $\varepsilon = 9.6\%$. Top: AFM profile; bottom: SWLI profile. The x direction is parallel to the direction of the tensile axis. After Zaiser et al. (2004).

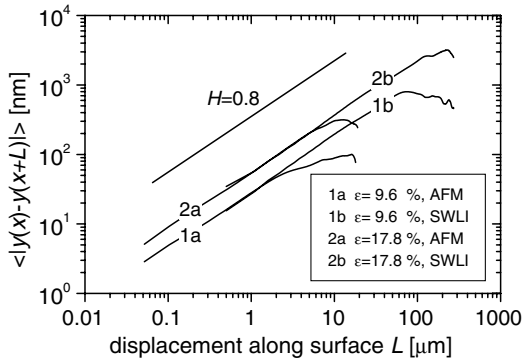

Fig. 2. Roughness plots (mean height difference vs. distance along the profile) for AFM and SWLI profiles obtained at strains of 9.6% and 17.8%. The corresponding profiles for $\varepsilon = 9.6\%$ are shown in Fig. 1.

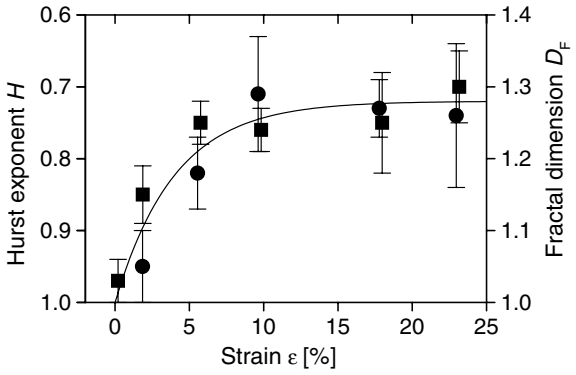

Fig. 3. Fractal dimension and Hurst exponent as a function of strain. Squares: values determined from scanning interferometry profiles. Circles: values determined from AFM profiles; each value represents an average over five profiles. Full line: guide to the eye.

percent of strain and then saturates at $D_B \approx 1.25$ (Fig. 3). Accordingly, the dimension of the surface itself is expected to be $D_B \approx 2.25$. Meissner et al. (1998) used scanning electron microscopy to investigate the surface of deformed Ni single and polycrystals; they report slightly higher surface dimensions $D_B \approx 2.5$.

Information about the temporal dynamics of plastic flow can be obtained from acoustic emission measurements. Measurements on ice single crystals reported by Weiss and Grasso (1997) and Miguel et al. (2001) indicate an intermittent acoustic signal composed of discrete 'events' with a scale-free size distribution. The probability density to observe events with energy release E decreases according to $p(E) \propto E^{-1.6}$ (Fig. 4). This observation indicates that plastic deformation proceeds in avalanches with a power-law size distribution reminiscent of the power-law distributions observed in many systems close to critical points.

The present paper is devoted to an extension of deterministic gradient constitutive models in order to capture spontaneous localization and avalanche dynamics of plastic deformation on mesoscopic scales. To describe inhomogeneity and jerkiness of plastic flow in spite of a convex macroscopic stress–strain law, it is necessary to allow for local deviations

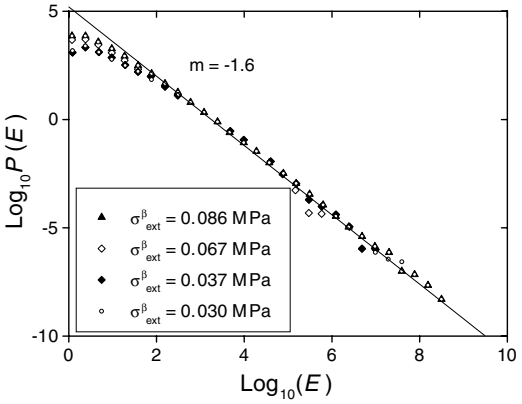

Fig. 4. Distribution of energy release in acoustic emission 'events' recorded during creep deformation of ice single crystals; temperature $T = 263$ K, resolved shear stresses on the basal plane as indicated in the inset. After Miguel et al. (2001).

from the overall macroscopic behavior by properly introducing fluctuations in the constitutive equations. This has been known for a long time in slip line theory, where one has to assume some local softening mechanism which is responsible for the initiation of a slip line. Accordingly, we envisage the interplay between local softening and hardening processes in terms of statistical fluctuations of the local flow stress. Fluctuations in the local flow stress lead to strain fluctuations which, in turn, give rise to long-range stress redistribution which can be expressed in terms of an elastic Green's function. Furthermore, dislocation–dislocation correlations give rise to a local back stress, which can be expressed in terms of the second-order strain gradient. These ideas are detailed in Section 2 where a gradient-dependent plasticity model enhanced with stochastic terms is presented. The model is constructed as to describe the interplay between gradient deterministic terms and stochastic terms in a simple, yet physically motivated manner. In Section 3, the numerical procedure employed to evaluate the model is briefly outlined. In Section 4, we discuss the results obtained from the numerical implementation of the model. We demonstrate that it correctly accounts for the observed statistics of 'slip avalanches', the pattern formation and arrangements of slip lines, as well as the corresponding deformation-induced surface morphology.

Finally, in Appendix A, we list technical details pertaining to fluctuations and statistical aspects of internal stress as determined by the underlying dislocation dynamics. This was done not only for the convenience of the reader who may not be familiar with basic concepts of statistical physics, but also for not destructing the presentation of the main ideas with unnecessary technicalities.

2. Plastic flow in dislocated crystals: a gradient plasticity model with disorder

To arrive at a physically motivated model of plastic flow in a crystalline solid, we start out from a microscopic description of plasticity in terms of the stress-driven motion of discrete lattice dislocations. For simplicity, we envisage straight parallel dislocations moving in a single slip system under the action of the local resolved shear stress. This local driving stress results both from the externally applied stress and from the internal stress created by

the dislocation arrangement. As discussed in detail in Appendix A, the internal stress (resolved shear stress) acting on a dislocation at a location $\boldsymbol{r}$ is the sum of an average internal stress $\langle\tau^d_{\rm int}(\boldsymbol{r})\rangle$ and a fluctuating internal-stress contribution $\delta\tau(\boldsymbol{r})$. The average internal stress $\langle\tau^d_{\rm int}(\boldsymbol{r})\rangle = \langle\tau_{\rm int}(\boldsymbol{r})\rangle + \tau_{\rm cor}(\boldsymbol{r})$ is made up of two contributions:

(i) $\langle\tau_{\rm int}(\boldsymbol{r})\rangle$ is the average internal stress at a generic point in space. It is related to the average strain γ (shear strain on the slip system under consideration) via the relationship

$$\langle\tau_{\rm int}\rangle = \frac{1}{b}\int \nabla_x\gamma(\boldsymbol{r}')\tau(\boldsymbol{r}-\boldsymbol{r}')\,\mathrm{d}^2\boldsymbol{r}', \tag{1}$$

where b is the modulus of the Burgers vector and τ is the shear stress created by a positive edge dislocation. This term describes the long-range stresses arising from strain incompatibilities and is discussed in more detail in Appendix A.

(ii) The term $\tau_{\rm cor}(\boldsymbol{r})$ takes into account the effect of dislocation–dislocation correlations. Because of such correlations, the stress at a point occupied by a dislocation is not the same as the stress at a generic point in space. This term can be approximated as a second-order gradient of the average strain via the relationship

$$\tau_{\rm cor}(\boldsymbol{r}) = \frac{DG}{\rho}\frac{\partial^2\gamma}{\partial x^2}, \tag{2}$$

where ρ is the total dislocation density, G is the shear modulus, and D is a numerical constant of the order of unity, as detailed in Appendix A. In fact, relations of the form of Eqs. (1) and (2) have been discussed briefly by Aifantis (2003) and in more detail by Groma et al. (2003) in an effort to show how collective dislocation dynamics arguments can lead to the appearance of strain gradients (see also Zaiser and Aifantis, 2003a,b). Similar arguments have been employed earlier (Zaiser and Aifantis, 1998, 1999) to justify the dependence of flow stress on second-order gradients in strain and/or dislocation densities. More recently, gradient terms have been incorporated into a statistical mechanics description of the collective behavior of dislocations coupled to standard small-strain continuum kinematics for single slip; and the resulting model has been successfully applied to obtain quantitative predictions of size effects in constrained plastic flow in metal-matrix composites, as well as in micro-bending (Yefimov et al., 2004a,b). In passing, it is noted that the above attempts were initially motivated by the W-A model (Walgraef and Aifantis, 1985a,b) which incorporated gradient terms in the equations of dislocation dynamics to consider dislocation patterning phenomena that could not be described by existing dislocation theories. This model, which is revisited in a subsequent paper of this volume (Pontes et al., 2006), has also motivated a large number of papers on discrete dislocation simulations, as an alternative approach to dislocation patterning (Kubin and Lepinoux, 1988).

As a dislocation moves through the internal stress field, it experiences an additional spatially fluctuating stress $\delta\tau(\boldsymbol{r})$ which depends on the positions of the dislocations in its vicinity. The average of the fluctuating stress is zero, and the characteristic 'amplitude' of the internal-stress fluctuations in the vicinity of $\boldsymbol{r}$ is given, as shown in Appendix A, by the relationship

$$\langle\delta\tau(\boldsymbol{r})^2\rangle = KG^2b^2\rho(\boldsymbol{r})\ln(\xi/b), \tag{3}$$

where $K = 1/[4(1-\nu)^2]$ is another numerical constant of the order of unity (ν is Poisson's ratio), and $\xi \approx 1/\sqrt{\rho}$ is the characteristic range of dislocation–dislocation correlations, which defines a characteristic 'screening radius' for the dislocation stress fields. In fact,

the spatial correlation function of the fluctuating internal stress field is given by [Eq. (A.22)]

$$\langle \delta\tau(\boldsymbol{r})\delta\tau(\boldsymbol{r}+\boldsymbol{r}')\rangle = \langle \delta\tau(\boldsymbol{r})^2\rangle h(\boldsymbol{r}'), \tag{4}$$

where $h(\boldsymbol{r}')$ is a non-dimensional correlation function with characteristic range ξ ($\int h(\boldsymbol{r})d^2r \approx \xi^2$). The derivation of Eqs. (3) and (4) is discussed in detail in Appendix A. A derivation for multiple-slip conditions, including an explicit expression which relates the stress correlation function $h(\boldsymbol{r})$ to the dislocation–dislocation correlation function, has been given by Zaiser and Seeger (2002) who also discuss the possibility to directly acquire experimental information on the statistics of fluctuating internal stresses from X-ray line profiles.

As discussed by Zaiser (2001), dislocations usually move in an extremely intermittent and jerky manner for typical experimental strain rates. In fact, the imposed deformation is brought about by the rapid motions of a very small number of dislocations, while the overwhelming majority of dislocations are practically at rest. It is, therefore, reasonable to envisage plastic flow in terms of the motion of individual dislocations through the fluctuating internal stress field created by the dislocations in their surroundings, and to approximate this stress field by that of a static dislocation arrangement. Since the fluctuating stresses are screened at distances of the order of $\xi \sim 1/\sqrt{\rho}$, this hypothesis simply means to assume that within a characteristic volume of linear size ξ only one dislocation is moving at a time. This approximation does not preclude the occurrence of collective dislocation motions, or 'slip avalanches', but simply implies that the dislocations moving in such avalanches are far apart and correlate over long, rather than short, distances.

In view of the above discussion, it follows that in the rate-independent limit, a dislocation moves as long as it experiences a positive local stress

$$\tau_{\text{ext}} + \langle \tau_{\text{int}}(\boldsymbol{r})\rangle + \frac{DG}{\rho}\frac{\partial^2\gamma}{\partial x^2} + \delta\tau(\boldsymbol{r}) > 0. \tag{5}$$

In other words, the positive local stress is made up by four contributions: the external stress, the average internal stress, the correlation stress, and the stress fluctuation term. We now adopt a coarse-grained description of plastic flow by spatially averaging over a volume $V_{\text{cg}} \approx \xi^2$. [Note that, since we are considering a two-dimensional system, V_{cg} has actually the dimension of an area.] We make the important assumption that the dislocation systems we are considering are *spatially ergodic* in the sense that we may interchange spatial and ensemble averages. In this case, the stress contributions $\langle \tau_{\text{int}}(\boldsymbol{r})\rangle$ and $\tau_{\text{cor}}(\boldsymbol{r})$, which can be expressed as functional of the ensemble-averaged strain, are invariant under spatial coarse-graining. The same holds for the external stress τ_{ext}.

We next consider the term $\delta\tau(\boldsymbol{r})$. To evaluate this term, we note that the coarse-graining volume is so small that within V_{cg} only one dislocation is moving at a time. Hence, the stress required to deform the volume element under consideration corresponds to the stress needed to move one single dislocation through this volume element. The distance s travelled by this dislocation can be related to the local strain γ via $\mathrm{d}\gamma = b\,\mathrm{d}s/V_{\text{cg}}$. Accordingly, we can interpret the fluctuating internal stress acting on the moving dislocation as a fluctuating "flow stress" $\delta\tau(\gamma,\boldsymbol{r})$ with the following statistical properties

$$\langle \tau(\boldsymbol{r},\gamma)\rangle = 0; \quad \langle \delta\tau(\boldsymbol{r},\gamma)\delta\tau(\boldsymbol{r}',\gamma')\rangle = \langle \delta\tau^2\rangle \xi^2 \delta(\boldsymbol{r}-\boldsymbol{r}')h(\gamma-\gamma'). \tag{6}$$

Here, $\langle \delta\tau^2 \rangle$ is given by Eq. (3) and the function h corresponds to the stress fluctuation correlation function taken in the direction of dislocation glide: $h(\gamma) = h(x = \gamma V_{cg}/b, y = 0)$. It goes to zero over a characteristic strain $\gamma_{cor} = b/\xi \approx b\sqrt{\rho}$.

The function $\delta(\boldsymbol{r} - \boldsymbol{r}')$ reflects the fact that the size of the coarse graining volume corresponds to the correlation length of stress fluctuations and, hence, fluctuations in different volume elements are statistically independent. The probability distribution of the random variable $\delta\tau$, finally, is approximately Gaussian (see Appendix A).

Combining the different stress contributions, we obtain the rate-independent constitutive equation (local stress equilibrium condition) in the form

$$\tau_{ext} + \frac{1}{b}\int \partial_x \gamma(\boldsymbol{r}')\tau(\boldsymbol{r} - \boldsymbol{r}')\,\mathrm{d}^2\boldsymbol{r}' + \frac{DG}{\rho}\frac{\partial^2\gamma}{\partial x^2} + \delta\tau(\gamma, \boldsymbol{r}) = 0. \tag{7}$$

This equation can be considered as a generalization of models used by Aifantis and coworkers (e.g., Aifantis, 2003, and references quoted therein) to describe strain localization phenomena in systems with non-convex stress–strain relationships. [For details, the reader can consult Aifantis (1987), as well as Zbib and Aifantis (1988, 1989, 1992).] In the present case $\delta\tau(\gamma, \boldsymbol{r})$ is a fluctuating function of the local strain γ, so again we have (locally) non-convex behavior and local instabilities. However, there are also important differences with respect to 'classical' plastic instabilities: (i) the local 'stress–strain relationship' $\delta\tau(\gamma, \boldsymbol{r})$ differs between different volume elements which are, however, coupled through the long-range and gradient stress terms, (ii) $\delta\tau(\gamma, \boldsymbol{r})$ has zero average both as a function of $\boldsymbol{r}$ and of γ. Nevertheless, the collective behavior of the interacting volume elements leads to a finite flow stress, as demonstrated below.

For later use, we note that we can obtain an alternative expression for the average internal stress $\langle \tau_{int} \rangle$. By using the stress field of an edge dislocation and integrating by parts, we may re-write $\langle \tau_{int} \rangle$ as

$$\langle \tau_{int}(\boldsymbol{r}) \rangle = \frac{Gb}{2\pi(1-\nu)}\int \gamma(\boldsymbol{r}')\left[\frac{1}{(\boldsymbol{r} - \boldsymbol{r}')^2} - \frac{8(x - x')^2(y - y')^2}{(\boldsymbol{r} - \boldsymbol{r}')^6}\right]\mathrm{d}^2\boldsymbol{r}' + \frac{G}{4(1-\nu)}[\bar{\gamma} - \gamma(\boldsymbol{r})], \tag{8}$$

where $\bar{\gamma}$ is the macroscopically averaged strain. The second term on the right-hand side of this equation is of a mean-field character: If only this term is considered, a volume element with larger than average strain experiences a back stress, and vice versa. The first term in Eq. (8), on the other hand, contains a kernel with zero angular average which effects an anisotropic stress re-distribution. [In the particular case where the strain $\gamma(\boldsymbol{r}')$ exceeds the average strain $\bar{\gamma}$ by a constant amount $\Delta\gamma$ within an ellipsoidal region, this term yields a spatially constant contribution within the ellipsoid such that Eq. (8) reduces to $\langle \tau_{int} \rangle = \Gamma\Delta\gamma$ where Γ is Eshelby's stress accommodation factor for an ellipsoidal inclusion.] As will be shown below, the mean-field term accounts for the observed statistics of slip avalanches, whereas the anisotropic term together with the gradient-dependent stress τ_{cor} is responsible for the formation of slip lines.

3. Numerical implementation

For numerical implementation we consider a slightly simplified version of the continuum model (Eq. (7)) which, however, preserves all the essential features of the competition

between gradient and stochastic terms. We use a lattice automaton technique where we discretize space in terms of a two-dimensional grid of cells, each cell representing a mesoscopic volume element of edge length $l \approx \xi$. This ensures that the fluctuating stresses in different volume elements are statistically independent. The local strains are discretized in units of the correlation strain $\gamma_{\mathrm{cor}} \approx b\sqrt{\rho}$. An infinite bulk system is mimicked by imposing periodic boundary conditions in both directions. The total dislocation density ρ and, hence, the statistical properties of the fluctuating internal stress field are assumed spatially homogeneous. A non-dimensional and dislocation density independent formulation is achieved by scaling all lengths in proportion with $\xi \approx 1/\sqrt{\rho}$, all stresses in proportion with $Gb\sqrt{\rho}/[2\pi(1-\nu)]$, and all strains in proportion with $b/\xi \approx b\sqrt{\rho}$.

The random function $\delta\tau(\gamma, \boldsymbol{r})$ in Eq. (7) is implemented as follows: to each volume element we assign initially a negative random value of $\delta\tau$ drawn from the negative half of a Gaussian distribution with mean square variation $\langle\delta\tau^2\rangle$ [Eq. (3)]. In physical terms, this implies that, initially, all dislocations are trapped in configurations where they are held up by negative (back) stresses. Whenever the net local stress on a volume element becomes positive, we increase the local scaled strain by a unit amount. We then assign a new random value of $\delta\tau$ to this volume element, which we chose again from a Gaussian distribution of mean square variation $\langle\delta\tau^2\rangle$. Since the fluctuating stresses acting on different volume elements are chosen independently, this procedure produces a random field with the required spatial correlations.

In each simulation run, we increase the applied stress τ_{ext} from zero in small increments $\Delta\tau_{\mathrm{ext}}$ until it reaches the yield stress of the weakest volume element. We then increase the local strain as discussed above and assign a new value of $\delta\tau$ to this volume element. Now we compute the internal stress field $\langle\tau_{\mathrm{int}}(\boldsymbol{r})\rangle$ using the periodically continued elastic Green's function of a two-dimensional isotropic medium, and evaluate the gradient-dependent stress contribution using the discrete second-order gradient. Once these internal stresses are computed, we check whether the stress acting on any other volume element exceeds now the local yield stress. In this case we again increase the local strain there and assign a new value to the yield stress. The process is repeated until all volume elements are stable, i.e., the local stress everywhere falls below the local yield stress, or until the average strain within the system exceeds a prescribed terminal strain at which we terminate our simulation. If the system settles into an equilibrium configuration before reaching the terminal strain, we increase the external stress by another amount $\Delta\tau_{\mathrm{ext}}$, and so on. The external driving is made adiabatically slow by choosing the external stress increment $\Delta\tau_{\mathrm{ext}}$ small enough such that the results of our simulations do not change if $\Delta\tau_{\mathrm{ext}}$ is further decreased.

4. Results

We first focus on the stress–strain response predicted by the model. To understand this behavior, it is important to note that in its present form the model does not contain any hardening mechanism. Thus, if the fluctuating stress in Eq. (7) is replaced by a space and strain-independent back stress (flow stress), the model would simply re-produce ideally plastic behavior in single-slip crystal plasticity.

However, the actual behavior of the system differs from ideal plasticity since the 'back stress' term in Eq. (7) is actually a fluctuating function of stress and strain with zero average. A stress–strain graph obtained from numerical simulation of this model is illustrated in Fig. 5. In order to realize the orders of magnitude involved, one may revert

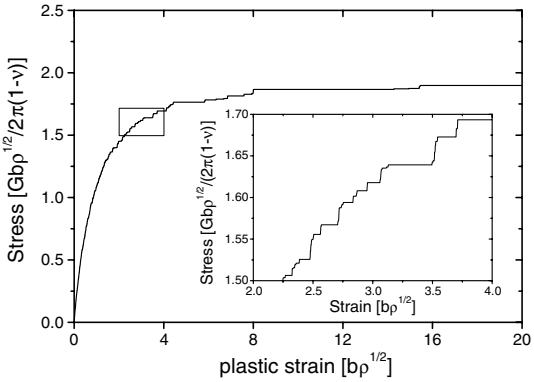

Fig. 5. Stress–strain curve as obtained from simulation of a system with 128×128 sites. Inset: detail of the same stress–strain graph.

two-dimensional variables using typical parameters at the onset of deformation of pure Cu single crystals: $G = 40$ MPa, $\nu = 0.3$, $b = 2.5 \times 10^{-10}$ m, $\rho = 10^{12}$ m^{-2}, and $\xi = 1/\sqrt{\rho} = 10^{-6}$ m. With these parameters, the scaled stress and strain ranges visible in Fig. 5 correspond to $0 \leqslant \tau_{\text{ext}} \leqslant 6$ MPa and $0 \leqslant \langle\gamma\rangle \leqslant 0.5\%$, respectively. The figure can, hence, be thought of as describing the microplastic region and yielding transition at the onset of easy-glide deformation in fcc single crystals.

From Fig. 5, the following observations can be made: (i) in spite of the fact that the averages of $\delta\tau$ over γ at fixed $\boldsymbol{r}$ (or over $\boldsymbol{r}$ at fixed γ) are zero, a finite stress (yield stress) of $\tau_c \sim 1.9$ (in scaled coordinates) is required to sustain deformation. This is because the local strains in the different volume elements are not equal: the system is trapped in 'strong' configurations where local strains are such that $\delta\tau$ is negative in most volume elements, thereby creating a non-zero average back stress, (ii) the yield stress is approached asymptotically through a 'microplastic' region where weak configurations are gradually eliminated, (iii) the increase of plastic strain with increasing stress occurs in discrete 'slip avalanches' of varying size. The intervals between the larger avalanches divide into avalanches of smaller size, and the characteristic avalanche size diverges as one approaches the yield stress. Before investigating in detail the micro-instabilities which manifest themselves in terms of these slip avalanches, we first study the *average* behavior that can be deduced from the simulations. To this end we average the stress–strain graphs over a large number of simulations to obtain a (nearly) smooth stress–strain relationship (Fig. 6).

From the semi-logarithmic plot, we find a logarithmic divergence of the strain as $\tau_{\text{ext}} \to \tau_c$ – in other words, the yield stress τ_c is approached exponentially. Accordingly, the stress susceptibility $\chi = \partial\gamma/\partial\tau_{\text{ext}}$ of the plastic strain diverges as we approach the yield stress:

$$\chi \propto (\tau_c - \tau_{\text{ext}})^{-\theta}, \tag{9}$$

where the critical exponent $\theta \approx 1$. We now investigate in more detail the 'strain bursts' that manifest themselves as stepwise strain increments in the individual stress–strain graphs. To this end, we record the strain increments (if any) occurring after each stress increment $\Delta\tau_{\text{ext}}$. Since the total strain increment due to a slip avalanche depends on the system size V_s (a given local slip avalanche produces a smaller total strain increment $\Delta\Gamma$ in a larger

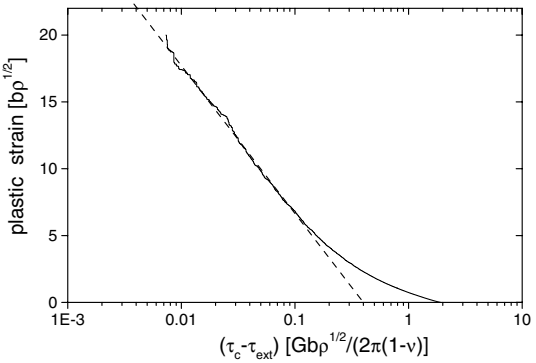

Fig. 6. Ensemble-averaged stress–strain graph as obtained by averaging over 60 simulations of systems with 128×128 sites. Strain is plotted against distance from the critical stress.

system), we characterize the avalanche sizes in terms of the dissipated energy $\Delta E = \tau_{\mathrm{ext}} V_s \Delta \Gamma$ which is proportional to the strain increment but does not depend on system size. We then determine the probability distribution of avalanche sizes within different external stress intervals, corresponding to different distances from the critical stress τ_C. Results are given in Fig. 7 where energy release distributions are compiled that have been obtained from simulations of an ensemble of systems of 256×256 sites.

It is seen that the distributions exhibit a power-law decay $p(\Delta E) \propto \Delta E^{-k}$ which is truncated at a characteristic burst size ΔE_c. The exponent $k = 1.4 \pm 0.1$ is in reasonable agreement with the experimental value $k = 1.6$ reported in the introduction. An exponent $k < 2$ implies that the first moment of the distribution is governed by the upper truncation limit, $\langle \Delta E \rangle \propto \Delta E_c^{2-k}$.

As the stress approaches the critical stress, this upper limit is expected to diverge, leading to a divergence of the average burst size. Indeed, it turns out that energy release distributions obtained at different applied stresses can be collapsed into a single universal

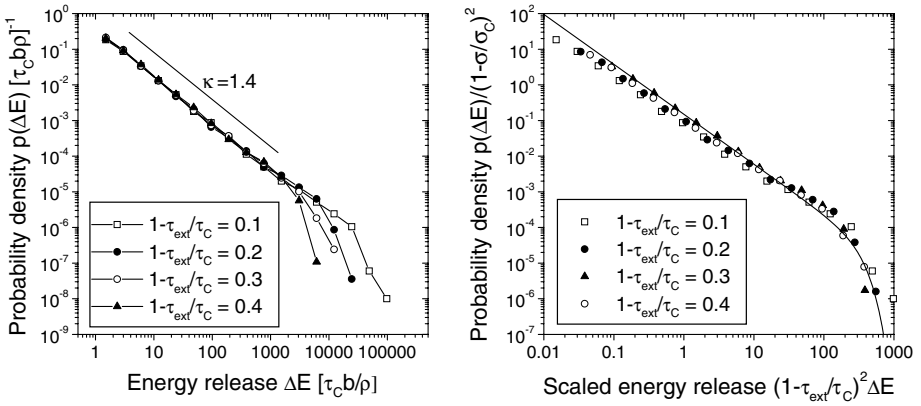

Fig. 7. Probability distributions of slip avalanche sizes (probability density $p(\Delta E)$ vs. energy release ΔE) as obtained from an ensemble of systems of size 256×256. (Left) Distributions corresponding to different stresses. (Right) Universal distribution obtained by re-scaling $\Delta E \to \Delta E(1 - \tau_{\mathrm{ext}}/\tau_c)^2$; full line: theoretical curve (Eq. 10).

distribution if the energy releases are re-scaled by a factor $(1-\tau_{ext}/\tau_c)^{1/\sigma}$ where τ_{ext} is the stress at which the distribution has been obtained and $\sigma \approx 0.5$ (Fig. 7, right).

The results for the susceptibility and the avalanche statistics are not independent from each other since the susceptibility is proportional to the average burst size. We therefore expect the susceptibility to diverge like $\chi \propto (\tau_c - \tau)^{-(2-k)/\sigma}$. With $k \approx 1.4$ and $\sigma \approx 0.5$ we find $\theta = (2-k)/\sigma \approx 1$, in reasonable agreement with Eq. (9). A theoretical framework for understanding the behavior observed in the simulations is provided by the theory of elastic interface depinning. In fact, the mean-field version of the present continuum model is equivalent to the mean-field model of a depinning interface as discussed, for example, by Fisher (1998) and Zapperi et al. (1998). The theoretical exponents for the mean-field model of a depinning interface are $\theta = 2$, $\sigma = 0.5$ and $k = 1.5$, in good agreement with the present simulation results. The theoretically predicted avalanche size distribution for mean-field depinning is

$$p(\Delta E) \propto \Delta E^{-1.5} \exp\left[-\left(\frac{\Delta E}{\Delta E_c}\right)^2\right], \tag{10}$$

which again compares well with the results of the simulations (Fig. 7).

The theory of elastic interface depinning allows us to envisage slip avalanches in plastic flow within a general theoretical framework which encompasses also avalanche phenomena in the motion of magnetic domain walls (Barkhausen noise, Zapperi et al., 1998), the dynamics of earthquakes or the motion of cracks (Fisher, 1998). Already in a mean-field approximation, the theory provides a framework for understanding the size distribution of slip avalanches and the behavior of the stress–strain curves as one crosses the microplastic region and approaches the yield stress. However, a mean-field model may not account, in principle, for the observed anisotropic spatial distribution of slip, the formation of slip lines, and the development of a self-affine surface morphology.

Fig. 8 shows a grey-scale representation of the strain pattern $\gamma(x,y)$ that emerges in a typical simulation. One observes a 'slip-line'-pattern with pronounced correlations along the direction of the slip plane (x direction in Fig. 8). Such stratified slip patterns are commonly observed in single-slip crystal plasticity experiments. They are a natural

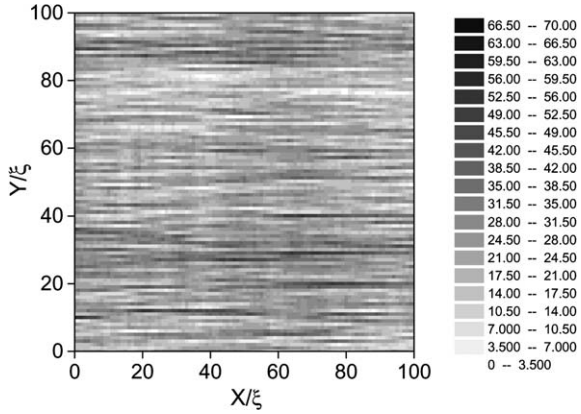

Fig. 8. Strain pattern obtained after simulation of a system of size 256×256 to an average strain of $20b\sqrt{\rho}$ (slip direction from left to right); greyscale: local strain in units of $b\sqrt{\rho}$.

consequence of the directed glide of lattice dislocations along the slip lanes. It is, however, remarkable to note that the present gradient plasticity model enhanced with stochastic terms, is capable of accounting for these features since we do not explicitly account for the motion of lattice dislocations. In fact, the only term in our model that distinguishes the direction of slip from the direction of the slip plane normal stems from the gradient-dependent stress contribution in Eq. (7) which tends to homogenize the slip pattern along the direction of slip. If this term is left out, the 'slip-line' patterns as shown in Fig. 8 disappear.

We now proceed to evaluate the surface profiles which correspond to the simulated slip patterns. We consider a surface which intersects the slip plane at a normal angle running along the plane $x = 0$. The displacement u in the direction normal to the surface fulfills the relationship

$$\frac{\partial u}{\partial y} = \gamma(x = 0, y), \tag{11}$$

This can be understood as the sum of a displacement due to the macroscopically averaged strain $\bar{\gamma}$, which leads to a rigid rotation of the surface, plus a random displacement due to the strain fluctuation $\delta\gamma(x = 0, y) = \gamma(x = 0, y) - \bar{\gamma}$. The surface profile may be obtained by direct integration of the strain fluctuation,

$$h(y) = \int_0^y [\gamma(x = 0, y') - \bar{\gamma}]\mathrm{d}y'. \tag{12}$$

A surface profile obtained in this manner is shown in Fig. 9.

We now proceed to assess the simulated profiles in terms of their roughness exponent. To this end, we use a procedure similar to that shown in Fig. 2; i.e., we plot the mean square height difference $\langle|u(x) - u(x + l)|\rangle$ between two points along the profile as a function of their separation l. For a self-affine profile we expect $\langle|u(x) - u(x + l)|\rangle \propto l^H$ where H is the Hurst exponent. Fig. 10 demonstrates that our simulated profiles are indeed self-affine with a Hurst exponent $H \approx 0.7$. Increasing the total strain leads to an increase in the absolute magnitude of surface height variations but does not change the Hurst exponent. Both the numerical value of the Hurst exponent and its strain independence compare favorably with the experimental observations quoted in Section 1.

To discuss the implications of a self-affine surface morphology with Hurst exponent $H = 0.7$, we note that the Hurst exponent of a self-affine random graph $u(y)$ is related to the correlation function of the derivative $\partial u/\partial y$; i.e., to the correlation function of

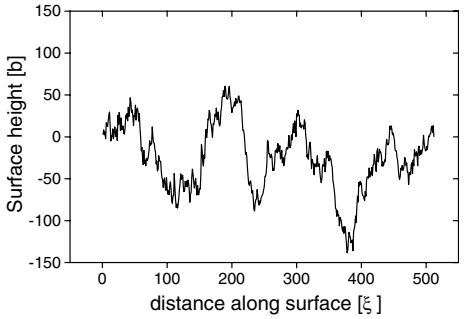

Fig. 9. Surface profile obtained from a system of size 512×512 after simulation to an average strain of $\bar{\gamma} = 20b\sqrt{\rho}$.

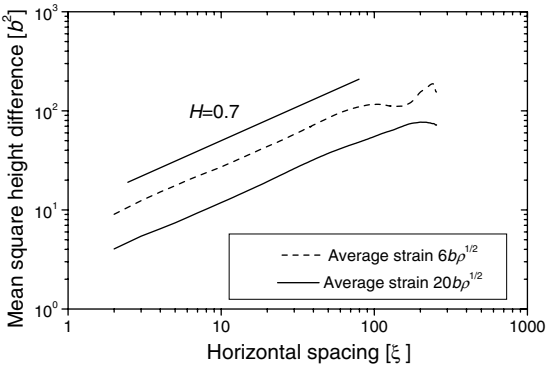

Fig. 10. Mean square height difference vs. horizontal distance for surface profiles obtained from a system of size 512×512 after simulation to average strains of $6b\sqrt{\rho}$ and $20b\sqrt{\rho}$; each graph has been averaged over 10 simulated profiles.

the strain fluctuations. Specifically, a Hurst exponent $H > 0.5$ indicates the presence of long-range correlations which decay in space according to the power-law relationship

$$\langle \delta\gamma(y)\delta\gamma(y+l)\rangle \propto l^{2H-2}. \tag{13}$$

The presence of long-range correlations implies that strain fluctuations average out more slowly than expected according to Gaussian statistics. Specifically, the magnitude of strain fluctuations averaged over the scale L decreases like

$$\langle \delta\gamma(y)^2\rangle L \approx \langle \delta\gamma(y)^2\rangle \xi \left[\frac{\xi}{L}\right]^{2-2H}, \tag{14}$$

where $\langle \delta\gamma(y)^2\rangle \xi$ is the magnitude of strain fluctuations on the scale of the stress fluctuation correlation length ξ. For $H = 0.7$, this implies that the average fluctuations decrease like $L^{-0.3}$ only as one increases the averaging volume. To give an order of magnitude of the effect, we determine the magnitude of the local strain fluctuations in our simulation. We find that $\langle \delta\gamma(y)^2\rangle \xi / \langle\gamma\rangle^2 = 0.25$ after simulation to a strain of $\langle\gamma\rangle = 20b\sqrt{\rho}$. With $\xi \approx \rho^{-1/2}$ and for a typical value of $\rho = 10^{12}\ \mathrm{m}^{-2}$ we find that the relative strain fluctuations are still on the order of 6% after averaging over a on a length of $L = 1$ mm. This observation explains why it is possible to detect significant strain fluctuations even on macroscopic scales (Zaiser and Hähner, 1996).

5. Discussion and conclusions

Our simulations demonstrate that it is possible to capture most essential aspects of slip avalanches in terms of a simple continuum model. By combining a fluctuating local stress–strain relationship with a strain-gradient dependent stress contribution and long-range stresses mediated by the elastic Green's function, the model accounts both for the observed spatial heterogeneities of plastic deformation (slip lines, self-affine surface roughness) and the emergence of 'bursts' of plastic activity with a power-law size distribution. Nevertheless, there are still several related questions that need to be studied: (i) Is it possible to formulate a dislocation-based model which exhibits the same behavior? (ii) In its present formulation the model does not account for hardening processes, as the statistical properties

of the internal-stress field are assumed to be strain-independent. On the other hand, Zaiser and Aifantis (2003a,b) have shown for a simplified one-dimensional model that hardening may delimit the size of slip avalanches. Should a similar effect be expected here? (iii) How does the behavior of the model change if we allow for slip on multiple slip systems and three-dimensional slip patterning?

While further work is required to investigate these issues, we may note already at this point that the present results demonstrate that fluctuation phenomena in plastic flow exhibit strong analogies with problems that have been studied in the physics of random or disordered systems. In particular, the concepts of randomness and disorder may apply to crystalline materials when the plastic flow resistance is governed by the existence of a random microstructure (here: a random dislocation pattern). Even though the present model explicitly accounts for the crystallographic slip that is imposed by the crystal lattice structure, it has also strong analogies with models employed to describe the plasticity of amorphous materials (Baret et al., 2002). Such analogies are not incidental but arise naturally as a consequence of the universal properties that characterize the driven dynamics of heterogeneous media – irrespective of whether one is dealing with earthquakes (Chen et al., 1991), amorphous materials (Baret et al., 2002) or, as in the present case, with crystal plasticity. In this connection, the reader is referred to a future paper (Moretti et al., forthcoming) where a three-dimensional extension of the model outlined here is presented, and to a forthcoming more general review-like article (Zaiser and Aifantis, forthcoming), where this issue and example problems of plastic instabilities and deformation patterning will be discussed in connection with the approach of driven dynamics of heterogeneous media.

Acknowledgements

Financial support by the European Commission under RTN/DEFINO HPRN-CT 2002-00198 and of EPSRC under Grant No. GR/S20406/01 is gratefully acknowledged. We also thank Mikko Alava and Stefano Zapperi for many stimulating discussions on problems of interface depinning.

Appendix A. Statistical treatment of internal stresses in dislocated crystals

A.1. Single slip configuration and dislocation densities

We envisage a system of straight parallel dislocations on a single slip system. The restriction to a single slip system serves only to keep the notation simple and the presentation instructive. It can be relaxed without affecting in any way the subsequent argument; a more detailed discussion which allows for an arbitrary number of slip systems and dislocations of general type has been given by Zaiser and Seeger (2002). The location of the ith dislocation is denoted by $\boldsymbol{r}_i$ and its sign by s_i ($s_i \in [1,-1]$ or $s_i \in [+,-]$). The internal stress at the point $\boldsymbol{r}$ is then given by the relation

$$\tau_{\mathrm{int}}(\boldsymbol{r}) = \sum_i s_i \tau(\boldsymbol{r} - \boldsymbol{r}_i). \tag{A.1}$$

For simplicity, we consider only the resolved shear stress on the given dislocation slip system; the generalization to other components of the internal stress tensor is possible, but not necessary for the subsequent discussion.

To investigate the statistical properties of the internal stress field, we formally characterize the dislocation arrangement by the discrete densities

$$\rho_{\mathrm{D}}^{s} = \sum_{i} \delta(\boldsymbol{r} - \boldsymbol{r}_i)\delta_{ss_i}, \tag{A.2}$$

where the Dirac delta function $\delta(\boldsymbol{r} - \boldsymbol{r}_i)$ localizes the density function at the dislocation positions and the Kronecker-Delta δ_{ss_i} ensures that only dislocations of sign s count towards ρ_{D}^{s}. To define continuous sign-dependent dislocation densities $p^{s}(\boldsymbol{r})$,we envisage an ensemble of statistically equivalent dislocation systems and average over the ensemble:

$$\rho^{s}(\boldsymbol{r}) = \left\langle \sum_{i} \delta(\boldsymbol{r} - \boldsymbol{r}_i)\delta_{ss_i} \right\rangle. \tag{A.3}$$

In a similar manner, we may define dislocation pair densities

$$\rho_{(2)}^{ss'}(\boldsymbol{r}, \boldsymbol{r}') = \left\langle \sum_{i\#j} \delta(\boldsymbol{r} - \boldsymbol{r}_i)\delta(\boldsymbol{r}' - \boldsymbol{r}_j)\delta_{ss_i}\delta_{s's_j} \right\rangle, \tag{A.4}$$

and higher-order densities may be defined accordingly. The sign-dependent dislocation density $\rho^{s}(\boldsymbol{r})$ is the probability density to find, in a randomly chosen member of the ensemble, a dislocation of sign s at the location $\boldsymbol{r}$. Accordingly, the pair density $\rho_{(2)}^{ss'}(\boldsymbol{r}, \boldsymbol{r}')$ is the joint probability density to find dislocations of signs s and s' at the respective locations $\boldsymbol{r}$ and $\boldsymbol{r}'$. These pair densities can always be written as

$$\rho_{(2)}^{ss'}(\boldsymbol{r}, \boldsymbol{r}') = \rho^{s}(\boldsymbol{r})\rho^{s'}(\boldsymbol{r}')\left[1 + d^{ss'}(\boldsymbol{r}, \boldsymbol{r}')\right]. \tag{A.5}$$

This expression defines the dislocation pair correlation functions $d^{ss'}(\boldsymbol{r}, \boldsymbol{r}')$, which characterize the local arrangement of dislocations relative to each other. These correlation functions play a crucial role for the understanding of the statistics of dislocation-induced internal stresses. For weakly correlated dislocation arrangements (dislocation arrangements without long-range order in the individual dislocation positions), Zaiser et al. (2001b,a) and Zaiser and Seeger (2002) have demonstrated that the pair correlation functions have the following properties:

- Dislocation pair correlation functions are *short-ranged*, i.e., they decay for large values of $|\boldsymbol{r} - \boldsymbol{r}'|$ faster than algebraically.
- Their range ξ is about one average dislocation spacing, $\xi \approx 1/\sqrt{\rho}$, where $\rho = \sum_{s}\rho^{s}$ is the total dislocation density. This implies that the dislocation densities (which may be space-dependent on a larger scale) can be considered approximately constant over the typical range of dislocation pair correlations. In a local density approximation the correlation functions can, hence, be approximated by those of a homogeneous dislocation arrangement. In this case, they depend on the relative coordinate only and one may approximately write $d^{ss'}(\boldsymbol{r}, \boldsymbol{r}') = d^{ss'}([\boldsymbol{r} - \boldsymbol{r}'])\sqrt{\rho}$ with a parametric dependence on $\boldsymbol{r}$ through the slowly varying function $\rho = \rho(\boldsymbol{r})$.
- Pair correlations exhibit a *screening property* which for the system considered here can be written as

$$\sum_{s'} ss' \int \rho^{s'}(\boldsymbol{r}) d^{ss'}(\boldsymbol{r}, \boldsymbol{r}')\, \mathrm{d}^2 r' = -1 \quad \text{for all} \quad [s, \boldsymbol{r}]. \tag{A.6}$$

A physical interpretation of this property is that each dislocation in the correlated arrangement is surrounded by exactly one 'excess dislocation' of opposite sign. Paradoxically this condition, which ensures that the dislocation energy is finite, can be met even if dislocations of only one sign are present (Zaiser and Seeger, 2002).

A convenient method for determining pair correlation functions is to perform simulations of the discrete dislocation dynamics and exploit the fact that because of the limited range of the correlations it is sufficient to simulate comparatively small systems. Fig. A.1 shows pair densities (densities of pairs of the same and of opposite signs, respectively) obtained from simulations of dislocation dynamics in single glide (Zaiser et al., 2001b). Equal numbers of dislocations of both signs were initially placed at random, and pair densities were determined after relaxation of the dislocation system to an equilibrium configuration at zero external stress. Fig. A.1 shows a tendency of dislocations of the same sign to form walls where they arrange perpendicularly above each other, whereas dislocations

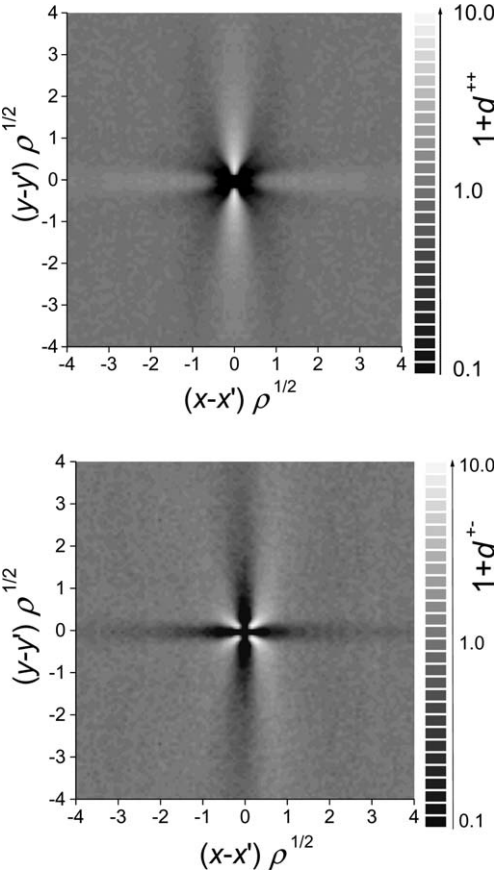

Fig. A.1. Pair correlation functions of dislocations of the same sign (top) and of opposite signs (bottom). The correlation functions pertain to a statistically homogeneous and stationary dislocation arrangement at zero external stress: They have been obtained by averaging over 50 2D simulations of systems consisting of 300 positive and 300 negative dislocations moving in a single slip system (after Zaiser et al., 2001b).

of opposite signs tend to form close dipoles with 45° orientations. At larger distances, correlations decay rapidly and no indications of long-range ordering are found.

A.2. Average internal stress and internal-stress fluctuations

We now evaluate the statistical properties of the internal-stress field in terms of dislocation densities and correlation functions. Since we are interested in a single-slip situation, we consider only the resolved shear stress component in the slip system under consideration. As a starting point, we write the internal stress at $\boldsymbol{r}$ in terms of the discrete dislocation densities ρ^s_{D}. In view of the definition given by Eq. (A.2), Eq. (A.1) is equivalent to

$$\tau_{\mathrm{int}}(\boldsymbol{r}) = \sum s \int \rho^s_{\mathrm{D}}(\boldsymbol{r}')\tau(\boldsymbol{r}-\boldsymbol{r}')\,\mathrm{d}^2 r. \tag{A.7}$$

The average internal stress at $\boldsymbol{r}$ follows by ensemble averaging. Using the definition given by Eq. (A.3), we obtain

$$\langle\tau_{\mathrm{int}}(\boldsymbol{r})\rangle = \int k(\boldsymbol{r}')\tau(\boldsymbol{r}-\boldsymbol{r}')\,\mathrm{d}^2 r. \tag{A.8}$$

Here, we have defined $k(\boldsymbol{r}) \equiv \rho^+(\boldsymbol{r}) - \rho^-(\boldsymbol{r})$ as the difference of the densities of positive and negative dislocations. This can be understood as a 'geometrically necessary' dislocation density, since it relates to the gradient of the average plastic strain $\gamma(\boldsymbol{r})$ via $k(\boldsymbol{r}) = (1/b)\nabla_x\gamma(\boldsymbol{r})$ where x is the dislocation glide direction.

Because of dislocation–dislocation correlations, the average stress $\langle\tau^d_{\mathrm{int}}(\boldsymbol{r})\rangle$ acting on a dislocation differs, in general, from the average internal stress at a generic point in space. Using the definitions and properties of the dislocation pair correlation functions discussed above, we may write

$$\langle\tau^d_{\mathrm{int}}(\boldsymbol{r})\rangle = \langle\tau_{\mathrm{int}}\rangle + \int \sum_{s'} s'\rho^{s}(\boldsymbol{r}')d^{ss'}(\boldsymbol{r}-\boldsymbol{r}')\tau(\boldsymbol{r}-\boldsymbol{r}')\,\mathrm{d}^2\boldsymbol{r}', \tag{A.9}$$

for a dislocation of sign s. We approximate the pair correlation functions by those for a homogeneous stress-free dislocation arrangement and note that in a statistically homogeneous dislocation arrangement the average stresses acting on positive and negative dislocations must be equal. With the definitions $\rho(\boldsymbol{r}) = \rho^+(\boldsymbol{r}) + \rho^-(\boldsymbol{r})$ and $k(\boldsymbol{r}) = \rho^+(\boldsymbol{r}) - \rho^-(\boldsymbol{r})$, and using the symmetry properties $d^{--} = d^{++}$ and $d^{+-} = d^{-+}$, the average stress acting on a dislocation is readily written as

$$\langle\tau^d_{\mathrm{int}}(\boldsymbol{r})\rangle = \langle\tau_{\mathrm{int}}\rangle + \int k(\boldsymbol{r}')d(\boldsymbol{r}-\boldsymbol{r}')\tau(\boldsymbol{r}-\boldsymbol{r}')\,\mathrm{d}^2\boldsymbol{r}', \tag{A.10}$$

where $d = d^{++} + d^{--} + d^{+-} + d^{-+}$. Now we use the fact that the dislocation pair correlation functions are short-ranged symmetrical functions with a range that scales in proportion with the dislocation spacing. By then expanding $\rho(\boldsymbol{r}')$ in Eq. (A.10) in a Taylor series around $\boldsymbol{r}' = \boldsymbol{r}$ and keeping only the lowest-order non-vanishing term (Groma et al., 2003), we have

$$\langle\tau^d_{\mathrm{int}}(\boldsymbol{r})\rangle \approx \langle\tau_{\mathrm{int}}\rangle + \frac{DG}{\rho}\partial_x k(\boldsymbol{r}'). \tag{A.11}$$

Because of the scaling properties of τ and d the quantity D defined in Eq. (A.11) by the integral $D \equiv \rho\int d(\boldsymbol{r})x\tau(\boldsymbol{r})\,\mathrm{d}^2\boldsymbol{r}$ does not depend on ρ. In evaluating Eq. (A.11) we have used

the symmetry properties $\tau(x,y) = \tau(x,-y) = -\tau(-x,y)$ and $d(x,y) = d(x,-y) = d(-x,-y)$ of the stress and pair correlation functions. According to Eq. (A.11), dislocation correlations lead to a correction term for the internal stress. This correction term is proportional to the second-order gradient of the average shear strain: Since $k = (1/b)\nabla_x\gamma$, the correction term has the form

$$\tau_{\mathrm{cor}}(\boldsymbol{r}) = \langle \tau^d_{\mathrm{int}}(\boldsymbol{r})\rangle - \langle \tau_{\mathrm{int}}\rangle = c\gamma_{xx}, \tag{A.12}$$

where the gradient coefficient c is defined as $c = DG/\rho$. In other words, this term yields a correction to the flow stress that is proportional to the second-order gradient of strain as proposed and discussed by Aifantis and co-workers (e.g., Aifantis, 2003, and references quoted therein).

As a dislocation moves through the internal-stress field, it experiences, in addition to the average stress, a fluctuating space-dependent internal-stress contribution. We denote the difference between the average stress and the actual stress at a given point in space as the internal-stress fluctuation, i.e.

$$\delta\tau(\boldsymbol{r}) = \tau_{\mathrm{int}}(\boldsymbol{r}) - \langle \tau_{\mathrm{int}}(\boldsymbol{r})\rangle. \tag{A.13}$$

The average stress depends on the average strain only and can, therefore, be readily treated in the usual way within a continuum model. Knowledge of the internal-stress fluctuations, on the other hand, requires, in principle, full information about the individual positions of all dislocations. The purpose of the subsequent statistical considerations is to extract statistical signatures of the internal-stress fluctuations (spatial correlations, probability density) which can be related to average properties of the dislocation system (average densities and correlation functions).

A.3. Internal-stress fluctuations: amplitude and spatial correlations

To characterize the spatial structure of the internal stress field, we evaluate the two-point correlation function

$$\langle \tau_{\mathrm{int}}(\boldsymbol{r})\tau_{\mathrm{int}}(\boldsymbol{r}')\rangle = \langle \tau_{\mathrm{int}}(\boldsymbol{r})\rangle\langle \tau_{\mathrm{int}}(\boldsymbol{r}')\rangle + \langle \delta\tau(\boldsymbol{r})\delta\tau(\boldsymbol{r}')\rangle. \tag{A.14}$$

This correlation function equals the product of the average stresses at $\boldsymbol{r}$ and $\boldsymbol{r}'$, plus the correlation function of the internal-stress fluctuations. Using the definitions given by Eqs. (A.4)–(A.6), we find that the latter is given by

$$\begin{aligned}\langle \delta\tau(\boldsymbol{r})\delta\tau(\boldsymbol{r}')\rangle &= \sum_s \int \rho^s(\boldsymbol{r}'')\tau(\boldsymbol{r}-\boldsymbol{r}'')\tau(\boldsymbol{r}'-\boldsymbol{r}'')\,\mathrm{d}^2r'' \\ &\quad + \sum_{ss'} \int\int ss'\rho^s(\boldsymbol{r}'')\rho^{s'}(\boldsymbol{r}'')d^{ss'}(\boldsymbol{r}'',\boldsymbol{r}''')\tau(\boldsymbol{r}-\boldsymbol{r}'')\tau(\boldsymbol{r}'-\boldsymbol{r}''')\,\mathrm{d}^2r''\,\mathrm{d}^2r''' \\ &= \sum_s \int\int \rho^s(\boldsymbol{r}'')[\delta(\boldsymbol{r}''-\boldsymbol{r}''') + f^s(\boldsymbol{r}''-\boldsymbol{r}''')]\tau(\boldsymbol{r}-\boldsymbol{r}'')\tau(\boldsymbol{r}'-\boldsymbol{r}''')\,\mathrm{d}^2r''\,\mathrm{d}^2r''',\end{aligned} \tag{A.15}$$

where, in the last step, we have defined the 'screening functions' f^s as $f^s(\boldsymbol{r}'',\boldsymbol{r}''') = \sum_{s'} ss'\rho^{s'}(\boldsymbol{r}'')d^{ss'}(\boldsymbol{r}'',\boldsymbol{r}''')$. As discussed above, because of the screening properties of dislocation pair correlations these functions have the property that $\int f^s(\boldsymbol{r}'',\boldsymbol{r}''')\,\mathrm{d}\boldsymbol{r}'' = -1$, which ensures that the stress-stress correlation function goes to zero for large $|\boldsymbol{r}-\boldsymbol{r}'|$.

Due to the short-range nature of the pair correlation functions, the screening functions are also short-ranged. This leads to short-ranged stress fluctuation correlations, with a range that is proportional to the range of dislocation pair correlations (see below). Hence, we can make the following simplifications: (i) we take the slowly varying dislocation density $\rho^s(\boldsymbol{r}'') \approx \rho^s(\boldsymbol{r})$ out of the integral in Eq. (A.11); (ii) we approximate the pair correlation functions by those for a homogeneous dislocation arrangement and write $f^s(\boldsymbol{r}'' - \boldsymbol{r}''') = \rho^{s'} \sum_{s'} s s' d_{ss'}(\boldsymbol{r}'' - \boldsymbol{r}''')$ where the weak $\boldsymbol{r}$ dependence of the dislocation density can be neglected over the range of the correlation function. Using these simplifications, the stress fluctuation correlation function can be represented as

$$\langle \delta\tau(\boldsymbol{r}) \delta\tau(\boldsymbol{r} - \boldsymbol{r}') \rangle = \sum_{\beta,s} \rho^s(\boldsymbol{r}) \int \int [\delta(\boldsymbol{r}'' - \boldsymbol{r}''') + f^s(\boldsymbol{r}'' - \boldsymbol{r}''')] \tau(\boldsymbol{r}''') \tau^\beta(\boldsymbol{r}'' - \boldsymbol{r}') \, \mathrm{d}^2 r'' \, \mathrm{d}^2 r'''. \tag{A.16}$$

The double convolution is conveniently evaluated in Fourier space. As a result, we find

$$\langle \delta\tau(\boldsymbol{r}) \delta\tau(\boldsymbol{r} - \boldsymbol{r}') \rangle = \sum_s \rho^s g^s(\boldsymbol{r}'), \tag{A.17}$$

where the Fourier transforms of the stress correlation functions $g^s(\boldsymbol{r})$ are given by

$$g^s(\boldsymbol{k}) = [1 - f^s(\boldsymbol{k})] \mid \tau(\boldsymbol{k}) \mid^2, \tag{A.18}$$

and $\tau(\boldsymbol{k})$ is the Fourier transform of the stress $\tau(\boldsymbol{r})$.

To assess the qualitative behavior of the stress fluctuation correlations, we study the simple case of equal dislocation densities $\rho^+(\boldsymbol{r}) = \rho^-(\boldsymbol{r}) = \rho(\boldsymbol{r})/2$ and a spherically symmetrical screening function $f^+(r) = f^-(r) = f(r)$. We calculate the angular average of $\langle \delta\tau(\boldsymbol{r}) \delta\tau(\boldsymbol{r} - \boldsymbol{r}') \rangle$ over the directions of $\boldsymbol{r}'$:

$$\langle \delta\tau(\boldsymbol{r}) \delta\tau(\boldsymbol{r} - \boldsymbol{r}') \rangle_\psi = \rho(\boldsymbol{r}) \bar{g}(\mid \boldsymbol{r}' \mid), \tag{A.19}$$

where the angular average $\bar{g}(\mid \boldsymbol{r} \mid) \equiv 1/(2\pi) \int g(\boldsymbol{r}) d\psi$ can be written as

$$\bar{g}(r) = KG^2 b^2 \int [1 - f(k)] \frac{1}{k} J_0(k|r'|) \, \mathrm{d}k. \tag{A.20}$$

Here, J_0 is the Bessel function, K is a non-dimensional numerical constant, and G is as usual the shear modulus. In deriving Eq. (A.20), we made use of the fact that the angular average of $|\tau(\boldsymbol{k})|^2$ can be written as $KG^2 b^2/(2\pi k)^2$ where $K = 1/[4(1 - \nu)^2]$. The result (A.20) may also be written as

$$\bar{g}(r) = KG^2 b^2 \int_r^\infty f(r') \ln[r'/r] 2\pi r' \, \mathrm{d}r'. \tag{A.21}$$

As an example, we consider the exponentially decaying pair correlation function $f(r) = 1/(2\pi[r_0]^2)\exp[-r/\xi]$ with range ξ, for which Eq. (A.21) yields $\bar{g}(r) = KG^2 b^2[\exp(-r/\xi) - \mathrm{Ei}(-r/\xi)]$ where $\mathrm{Ei}(x)$ is the exponential-integral function. Beyond $r \sim \xi$, the stress correlation function decays exponentially, monitoring the exponential decay of the dislocation pair correlations. This demonstrates that the stress correlation function is indeed short-ranged. For $r \to 0$, on the other hand, it exhibits a logarithmic divergence, $\bar{g}(r) \approx KG^2 b^2 \ln[\xi/r]$, which must be truncated at the dislocation core radius $r \approx b$. Using this truncation we may write the stress fluctuation correlation in the final form

$$\langle \delta\tau(\boldsymbol{r})^2 \rangle = KG^2b^2\rho(\boldsymbol{r})\ln[\xi/b],$$
$$\langle \delta\tau(\boldsymbol{r})\delta\tau(\boldsymbol{r}+\boldsymbol{r}')\rangle = \langle \delta\tau(\boldsymbol{r})^2\rangle h(\boldsymbol{r}'), \tag{A.22}$$

where $h(\boldsymbol{r}) = g(\boldsymbol{r})/(KG^2b^2\ln[\xi/b])$. Because of the general properties of dislocation pair correlations the correlation range ξ is proportional to the dislocation spacing, $\xi \sim \rho^{-1/2}$. Therefore, a density-independent representation of stress correlations is obtained by expressing all lengths in units of the average dislocation spacing. Fig. A.2 shows for three different directions the radial decay of the stress correlation function that has been calculated numerically from the dislocation pair correlation functions depicted in Fig. A.1. Again one observes a logarithmic behavior at small $r(r\sqrt{\varrho} \ll 1)$. At large distances the stress correlation function becomes anisotropic and decays to zero on a scale of the order of a few dislocation spacings. The numerical value of the screening length is less than one average dislocation spacing, $\xi\sqrt{\varrho} \approx 0.55$, reflecting the dipolar character of the dislocation arrangement.

A.4. Probability density function of internal stresses

The probability density function of the internal stress produced by the ensemble of dislocations, i.e., the probability $p(\boldsymbol{r},\tau)\,\mathrm{d}\tau$ to find at the position $\boldsymbol{r}$ the internal stress to be between τ and $\tau + d\tau$, has been calculated by Groma and Bako (1998). We briefly resume the main results of this work:

(i) The first moment of the local internal stress probability distribution is the mesoscopic internal stress $\langle \tau_{\mathrm{int}}(\boldsymbol{r})\rangle$. The distribution $p(\tau,\boldsymbol{r})$ is symmetrical around this value.
(ii) The tails of the distribution at large stresses depend only on the local dislocation density and are given by $p(\tau,\boldsymbol{r}) = [CG^2b^2\rho(\boldsymbol{r})]/\tau^3$ where C is a constant of the order of unity. These tails correspond to points in space which are very close to the dislocation lines (Zaiser and Seeger, 2002).

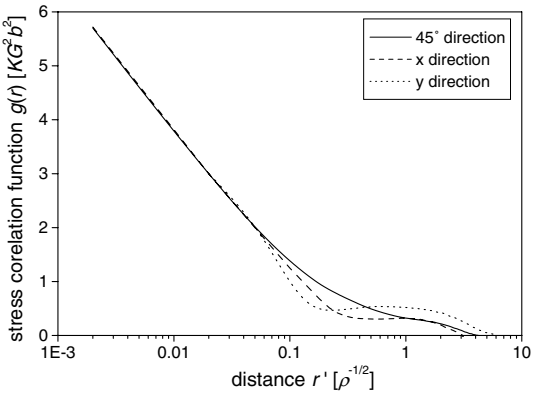

Fig. A.2. Radial decay of the two-point correlation function of internal-stress fluctuations for three different directions. The corresponding dislocation pair correlation functions are shown in Fig. A.1.

(iii) The shape and width of the central part of the distribution depend on the screening correlations in the dislocation arrangement. The half width of the distribution increases roughly in proportion with $\ln\xi/b$. For large screening radii the shape of the distributions approaches a Gaussian and the transition towards the fat tails where $p(\tau) \propto \tau^{-3}$ occurs at large stresses only.

Since the tails of the distribution correspond to locations very close to dislocation lines, they are not relevant for long-range dislocation motion, as dislocations in these locations are in narrow dipole configurations which do not contribute appreciably to plastic flow. We may therefore consider exclusively the central part of the internal-stress distribution which is determined by the superposition of the stress fields of many dislocations, leading to an approximately Gaussian shape of the distribution.

References

Aifantis, E.C., 1984. On the microstructural origin of certain inelastic models. J. Eng. Mater. Technol. 106, 326–330.

Aifantis, E.C., 1987. The physics of plastic deformation. Int. J. Plasticity 3, 211–247.

Aifantis, E.C., 1992. On the role of gradients in the localization of deformation and fracture. Int. J. Eng. Sci. 30, 1279–1299.

Aifantis, E.C., 1995. Pattern formation in plasticity. Int. J. Eng. Sci. 33, 2161–2178.

Aifantis, E.C., 1996. Non-linearity, periodicity and patterning in plasticity and fracture. Int. J. Non-linear Mech. 31, 797–809.

Aifantis, E.C., 1999. Gradient deformation models at nano, micro and macro scales. J. Eng. Mater. Technol. 121, 189–202.

Aifantis, E.C., 2001. Gradient plasticity. In: Lemaitre, J. (Ed.), Handbook of Mechanical Behavior Models. Academic Press, New York, pp. 291–307.

Aifantis, E.C., 2003. Update on a class of gradient theories. Mech. Mater. 35, 259–280.

Aifantis, K.E., Willis, J.R., 2004. Interfacial jump conditions in strain-gradient plasticity and relations of Hall–Petch type. In: Kounadis, A., Providakis, C., Exadaktylos, G. (Eds.), Proceedings of the Seventh National Congress on Mechanics, vol. II, Chania, Greece, June 24–26, 2004, pp. 372–377.

Aifantis, K.E., Willis, J.R., 2005. The role of interfaces in enhancing the yield strength of composites and polycrystals. J. Mech. Phys. Sol. 53, 1047–1070.

Baret, J.-C., Vandembroucq, D., Roux, S., 2002. An extremal model for amorphous media plasticity. Phys. Rev. Lett. 89, 195506.

Charalambakis, N., Aifantis, E.G., 1991. Thermoviscoplastic shear instability and higher order strain gradients. Int. J. Eng. Sci. 29, 1639–1650.

Chen, K., Bak, P., Obukhov, S.P., 1991. Self-organized criticality in a crack-propagation model of earthquakes. Phys. Rev. A 43, 625–630.

Fisher, D.S., 1998. Collective transport in random media: From superconductors to earthquakes. Phys. Rep. 301, 113–150.

Fleck, N.A., Hutchinson, J.W., 1993. A phenomenological theory for strain gradient effects in plasticity. J. Mech. Phys. Solids 41, 1825–1857.

Fleck, N.A., Hutchinson, J.W., 1997. Strain gradient plasticity. In: Hutchinson, J.W., Wu, T.W. (Eds.), Advances in Applied Mechanics. Academic Press, New York, pp. 295–361.

Fleck, N., Hutchinson, J.W., 2001. A reformulation of strain gradient plasticity. J. Mech. Phys. Solids 49, 2245–2271.

Fleck, N., Willis, J.R., 2004. Bounds and estimates for the effect of strain gradients upon the effective plastic properties of an isotropic two-phase composite. J. Mech. Phys. Solids 52, 1855–1888.

Fleck, N.A., Muller, G.M., Ashby, M.F., Hutchinson, J.W., 1994. Strain gradient plasticity: theory and experiment. Acta Metall. Mater. 42, 475–487.

Frantziskonis, G., Aifantis, E.G., 2002. On the stochastic interpretation of gradient-dependent constitutive equations. Eur. J. Mech. A 21, 589–596.

Gao, H., Huang, Y., Nix, W.D., Hutchinson, J.W., 1999. Mechanism-based strain gradient plasticity-I. Theory. J. Mech. Phys. Solids 47, 1239–1263.

Groma, I., Bako, B., 1998. Probability distribution of internal stresses in parallel straight dislocation systems. Phys. Rev. B 58, 2969–2974.

Groma, I., Csikor, F., Zaiser, M., 2003. Spatial correlations and higher-order gradient terms in a continuum description of dislocation dynamics. Acta Mater. 51, 1271–1281.

Gudmundson, P., 2004. A unified treatment of strain gradient plasticity. J. Mech. Phys. Solids 52, 1379–1406.

Gurtin, M.E., 2000. On the plasticity of single crystals: free energy, micro-forces, plastic strain gradients. J. Mech. Phys. Solids 48, 989–1036.

Gurtin, M.E., 2002. A gradient theory of single-crystal viscoplasticity that accounts for geometrically necessary dislocations. J. Mech. Phys. Solids 50, 5–32.

Huang, Y., Gao, H., Nix, W.D., Hutchinson, J.W., 2000. Mechanism-based strain gradient plasticity-II. Analysis. J. Mech. Phys. Solids 48, 99–128.

Kleiser, T., Bocek, M., 1986. The fractal nature of slip in crystals. Z. Metallkde. 77, 582–587.

Konstantinidis, A., Aifantis, E.G., 2002. Recent developments in gradient plasticity – part II: plastic heterogeneity and wavelets. J. Eng. Mater. Technol. 124, 358–364.

Kubin, L.P., Estrin, Y., Aifantis, E.G., 1993. Viewpoint set on propagative plastic instabilities. Scripta Metall. Mater. 29, 1147–1150.

Kubin, L.P., Lepinoux, J., 1988. The dynamic organization of dislocation structures. In: Kettunen, P.O. et al. (Eds.), Strength of Metal and Alloys, (ICSMA 8), 1. Pergamon Press, Oxford, pp. 35–59.

Maugin, G.A., Muschik, W., 1994. Themodynamics with internal variables. J. Non-Equil. Thermodyn. 19, 217–249, 250–289.

Meissner, O., Schreiber, J., Schwab, A., 1998. Formation of mesostructures at the surface of ferritic steel and a nickel monocrystal under increasing load – An in situ AFM experiment. Appl. Phys. A 66, S1113–S1116.

Menzel, A., Steinmann, P., 2000. On the continuum formulation of higher gradient plasticity for single and polycrystals. J. Mech. Phys. Solids 48, 1777–1796.

Miguel, M.C., Vespignani, A., Zapperi, S., Weiss, J., Grasso, J.-R., 2001. Intermittent dislocation flow in viscoplastic deformation. Nature 410, 667–671.

Moretti, P., Zaiser, M., Aifantis, E.G., forthcoming. Avalanche phenomena and deformation patterns in plasticity. [see also: Zaiser, M., Aifantis, E.C., forthcoming. Random effects and instabilities in gradient plasticity.]

Muhlhaus, H.B., Aifantis, E.G., 1991. A variational principle for gradient plasticity. Int. J. Solids Struct. 28, 845–857.

Neuhäuser, H., 1984. Slip-line formation and collective dislocation motion. In: Nabarro, F.R.N. (Ed.), Dislocations in Solids, vol. 4. North-Holland, Amsterdam, pp. 319–440.

Oka, F., Yashima, A., Adachi, T., Aifantis, E.G., 1992. Instability of gradient-dependent viscoplastic model for clay saturated with water and FEM analysis. Appl. Mech. Rev. 45, 140–148.

Oka, F., Yashima, A., Sawada, K., Aifantis, E.G., 2000. Instability of gradient-dependent elastoplastic model for clay and strain localization. Comput. Meth. Appl. Mech. Eng. 183, 67–86.

Polizzotto, C., Borino, G., 1998. A thermodynamics-based formulation of gradient-dependent plasticity. Eur. J. Mech. A 17, 741–761.

Pontes, J., Walgraef, D., Aifantis, E.C., 2006. On dislocation patterning: Multiple slip effects in the rate equation approach. Int. J. Plast.

di Prisco, C., Impomisato, S., Aifantis, E.G., 2002. A viscoplastic constitutive model for granular soils modified according to nonlocal and gradient approaches. Int. J. Numer. Anal. Meth. Geomech. 26, 121–138.

Triantafyllidis, N., Aifantis, E.G., 1986. A gradient approach to localization of deformation – I. Hyperelastic materials. J. Elasticity 16, 225–238.

Valanis, K.C., 1996. A gradient theory of internal variables. Acta Mech. 116, 1–14.

Valanis, K.C., 1998a. A gradient thermodynamic theory of self-organization. Acta Mech. 127, 1–23.

Valanis, K.C., 1998b. Diffusion potential and well-posedness in non-associative plasticity. Int. J. Solids Struct. 35, 5173–5188.

Valanis, K.C., 2000. Gradient field theory of material instabilities. Arch. Mech. 52, 817–838.

Vardoulakis, I., Aifantis, E.G., 1991. A gradient flow theory of plasticity for granular materials. Acta Mech. 87, 197–217.

Voyiadjis, G.Z., Deliktas, B., Aifantis, E.G., 2001. Multi-scale analysis of multiple damage mechanisms coupled with inelastic behavior of composite materials. J. Eng. Mech. 127, 636–645.

Walgraef, D., Aifantis, E.C., 1985a. Dislocation patterning in fatigued metals as a result of dynamical instabilities. J. Appl. Phys. 58, 688–691.

Walgraef, D., Aifantis, E.C., 1985b. On the formation and stability of dislocation patterns – Parts I–III. Int. J. Eng. Sci. 23, 1351–1358, 1359–1364; 1365–1372.

Weiss, J., Grasso, J.-R., 1997. Acoustic emission in single crystals of ice. J. Phys. Chem. B 32, 6113–6117.

Weiss, J., Marsan, D., 2003. Three-dimensional mapping of dislocation avalanches: clustering and space/time coupling. Science 299, 89–92.

Yefimov, S., Groma, I., Van der Giessen, E., 2004a. A comparison of a statistical-mechanics based plasticity model with discrete dislocation plasticity calculations. J. Mech. Phys. Solids 52, 279–300.

Yefimov, S., Groma, I., Van der Giessen, E., 2004b. Bending of a single crystal: discrete dislocation and nonlocal crystal plasticity simulations. Modelling Simul. Mater. Sci. Eng. 12, 1069–1086.

Zaiser, M., 2001. Statistical modelling of dislocation systems. Mater. Sci. Eng. A 309/310, 304–315.

Zaiser, M., Aifantis, E.C., 1998. On the dynamic interaction between moving dislocations. Appl. Phys. A 66, 393–397.

Zaiser, M., Aifantis, E.C., 1999. Materials instabilities and deformation patterning in plasticity. Recent Res. Devel. Metall. Mater. Sci., Research Signpost 3, 79–103.

Zaiser, M., Aifantis, E.G., 2003a. Geometrically necessary dislocations and strain gradient plasticity – a dislocation dynamics point of view. Scripta Mater. 48, 133–139.

Zaiser, M., Aifantis, E.C., 2003b. Avalanches and slip patterning in plastic deformation. J. Mech. Behavior Mater. 14, 255–270.

Zaiser, M., Hähner, P., 1996. Random aspects of macroscopic plastic deformation. Philos. Mag. Lett. 73, 369–375.

Zaiser, M., Seeger, A., 2002. Long-range internal stresses, dislocation patterning and work hardening in crystal plasticity. In: Nabarro, F.R.N., Duesbery, M.S. (Eds.), Dislocations in Solids, vol. 11. North-Holland, Amsterdam, pp. 1–100.

Zaiser, M., Marras, S.I., Nadgorni, E., Stunk, H.P., Aifantis, E.C., 2001a. Fractal dislocation patterning in plastically deformed NaCl polycrystals. Phys. Status Solidi A 185, R4–R5.

Zaiser, M., Miguel, M.-C, Groma, I., 2001b. Statistical dynamics of dislocation systems: The influence of dislocation–dislocation correlations. Phys. Rev. B 64, 224102.

Zaiser, M., Madani, F., Koutsos, V., Aifantis, E.C., 2004. Self-affine surface morphology of plastically deformed metals. Phys. Rev. Lett. 93, 195507.

Zapperi, S., Cizeau, P., Durin, G., Stanley, H.E., 1998. Dynamics of a ferromagnetic domain wall – avalanches, depinning and the barkhausen effect. Phys. Rev. B 58, 6353–6366.

Zbib, H.M., Aifantis, E.C., 1988. On the localization and postlocalization behavior of plastic deformation – I/II/III. Res. Mech. 23, 261–305.

Zbib, H.M., Aifantis, E.C., 1989. A gradient-dependent flow theory of plasticity: application to metal and soil instabilities. Appl. Mech. Rev. 42, 295–304.

Zbib, H.M., Aifantis, E.C., 1992. On the gradient-dependent theory of plasticity and shear banding. Acta Mech. 92, 209–225.

Zbib, H.M., Aifantis, E.C., 2003. Size effects and length scales in gradient plasticity and dislocation dynamics. Scripta Mater. 48, 155–160.